WHEEL\RAIL INTERACTION DUE TO PARAMETRIC EXCITATION

Traian MAZILU[1]

Interacţiunea roată-şină datorată excitaţiei parametrice este cauzată de rigiditatea dinamică a căii care variază de-a lungul distanţei dintre traverse. Este prezentat un model original pentru studiul interacţiunii roată/şină datorată excitaţiei parametrice. Calea este redusă la o şină rezemată pe semi-traverse. Şina este considerată ca o grindă Timoshenko uniformă infinită. Pentru mişcarea longitudinală a şinei, aceasta este tratată ca o bară infinită. Mişcările verticală şi longitudinală ale şinei sunt cuplate prin suporţii de şină. Roata este considerată ca un disc care se rostogoleşte fără alunecare pe şină. Soluţia ecuaţiilor de mişcare este obţinută prin aplicarea unei originale metode bazată pe funcţiile Green. Sunt calculate deplasările verticale şi forţa de contact roată/şină. Sunt prezentate influenţele vitezei roţii şi masei roţii.

Wheel/rail interaction due to parametric excitation is caused by the dynamic stiffness of the track which varies along the span length. An original model for the wheel/rail interaction due to parametric excitation is presented. The track is reduced to a rail supported by semi-sleepers. The rail is considered as a uniform infinite Timoshenko beam. For longitudinal dynamics, the rail is treated as an infinite bar. The vertical and longitudinal dynamics of the rail is coupled to the rail pads. The wheel is regarded as a disc which rolls without slip on the rail. The solution of the motion equations is obtained by using an original Green's functions method. The vertical displacements and the contact force wheel/rail are calculated. The influences of the wheel speed and wheel mass are presented.

Keywords: wheel, rail, parametric excitation, Green functions

1. Introduction

When a loaded wheel rolls without slip on a rail supported by sleepers and both are perfectly smooth and they have no defects, wheel/rail interaction is caused only by the varying dynamic stiffness due to the sleepers. This particular interaction behaviour is known as 'wheel/rail interaction due to parametric excitation' or as 'steady state interaction'.

During wheel/rail interaction due to parametric excitation, the wheel/rail relative displacement is caused by the periodical dynamic stiffness of the rail's discretely support and the contact force varies too. The dynamic force of wheel/rail contact is periodical and its own fundamental frequency equals the ratio

[1] Lecturer, Dept. of Railway Vehicles, University "Politehnica"of Bucharest, ROMANIA

between the speed and the span length. It is actually interesting to study the wheel/rail interaction due to parametric excitation because this interaction behaviour overlaps on the wheel/rail vibration induced by the roughness. The result is an amplitude modulated vibration, in which the carrier frequency is caused by roughness excitation and the modulated is given by the parametric excitation.

Wheel/rail interaction due to parametric excitation was studied in many papers. Nordborg [1] used the Green functions method to solve wheel/rail interaction. He described some aspects of wheel/rail interaction. For the studied case, the contact force peaks sharply precisely above the support points, followed by a short loss of wheel/rail contact, also for smooth rails. It is impossible to eliminate the vibrations of the rail pinned-pinned mode by removing surface roughness.

Wu and Thompson [2] have studied the parametric excitation of the wheel/track system. They have developed an equivalent time-varying model for the track, according to the space-varying receptance in a sleeper bay. This track model was combined with a wheel mass model; wheel/rail interaction due to parametric excitation was simulated. As they have shown, the contact force due to parametric excitation increases in magnitude with the wheel speed. Further, the contact force may be compared with that due to the roughness excitation, especially at low frequencies. The force spectrum presents many harmonics with a fundamental component at the sleeper-passing frequency, and the components around the pinned-pinned resonance frequency are at a higher level.

Hou et al [3] have studied the asymmetrical vehicle/track interaction. They applied a finite element model, and many vehicle/track interaction behaviours have been studied. They have detected an interesting resonant case vehicle/track, when the wavelength equals half of the sleeper spacing.

The study of wheel/rail interaction due to parametric excitation requires the time-domain analysis for the wheel/rail response. Many studies may be cited. Clark et al [4] have proposed an analytical model, considering a track discretely supported, for the numerical simulation of the wheel/rail corrugation dynamic interaction. Also, Nielsen and Igeland [5] have studied the vertical interaction between a bogie and the track in the presence of many different kinds of practical imperfection, using a track model with finite elements.

The current work comes with a different solution for solving the issue of wheel/rail interaction due to parametric excitation. The moving wheel on a discretely supported rail model was considered. The rail model is based on a mixed ‘Timoshenko beam/infinite bar on a discrete pad’ model [6, 7].

The equations of track motion are integrated using the Green functions method in an original manner, and both the complex and real Green function of the rail are used. Starting to the real Green functions of the rail, a Green matrix of

the track is assembled, and the wheel/rail interaction due to parametric excitation can be simulated for any time value.

The influences of the wheel speed and the wheel mass are studied and other aspects too (spectral issue, corrugated rail).

2. Mathematical model

In the following, an analytical model of the wheel/rail interaction due to parametric excitation has been developed (fig. 1). The model has three parts: the track, the wheel and wheel/rail contact.

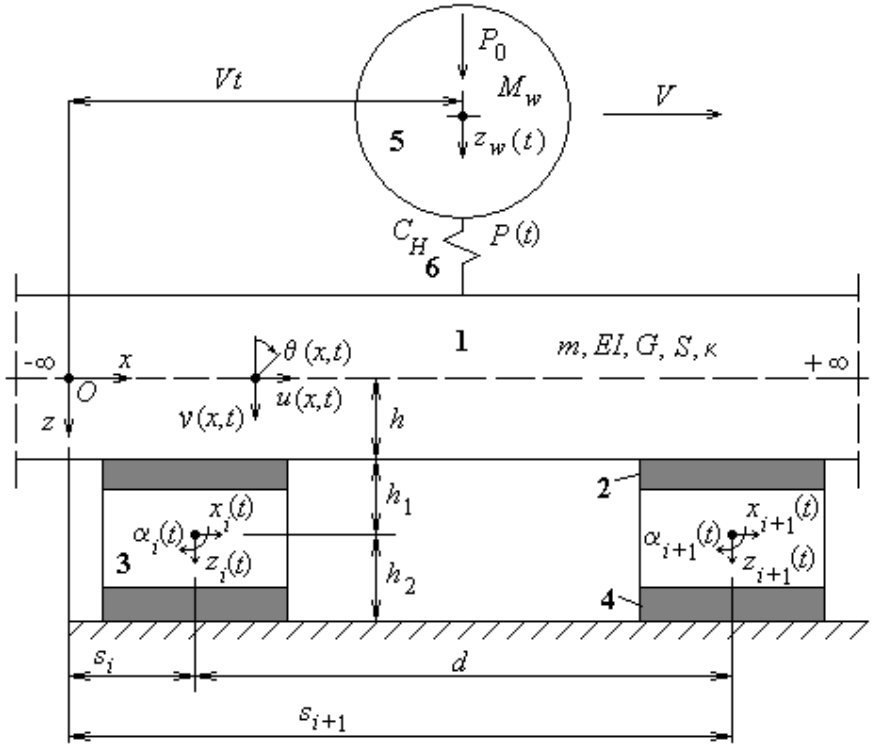

Fig. Mechanical model for wheel/rail interaction due to parametric excitation:
1. rail; 2. rail-pad; 3. semi-sleeper; 4. ballast; 5. wheel; 6. stiffness contact.

The track is reduced to a single rail discretely supported by semi-sleepers [7]. The rail is a uniform infinite Timoshenko beam with mass per length unit m. For longitudinal dynamics, the rail is treated as an infinite simple bar. The vertical and longitudinal dynamics of the rail is coupled to the rail pads. The parameters for the rail are: the Young's modulus E, the shear modulus G, the density ρ, the

cross-section area S, the area moment of inertia I and the shear coefficient κ. The distance from the rail foot to the cross – section neutral fibre is h. The loss factor of the rail is neglected. The dynamics of the rail are: the vertical displacement $v(x, t)$, the rotation of the cross-section $\theta(x, t)$ and the longitudinal displacement $u(x, t)$.

The rail pad is taken as a parallel connection of spring and dashpots having linear characteristics in x and z dimensions, and a similar torsion spring and damper restraining rotation in vertical-longitudinal plane. The elastic constants are k_{rx}, k_{rz} and $k_{r\alpha}$ and the viscous damping constants are c_{rx}, c_{rz} and $c_{r\alpha}$.

The ballast is modelled as a system of parallel connections of springs and dashpots having viscose damping in x and z dimensions. The elastic constants k_{bx}, k_{bz} and the viscous damping constants c_{bx}, c_{bz} are related to the ballast.

The semi-sleeper is considered as a rigid body with three degrees of freedom: the vertical translation $z_i(t)$, the lateral translation $x_i(t)$ (along the rail) and the rotation $\alpha_i(t)$ (across the rail). A semi-sleeper has the mass M_s and mass-moment of inertia I_s. The place of the sleeper i is s_i, and the span between the sleepers is d. The distances between the sleeper and the two elastic layers (modelling the rail pad and the ballast) are h_1 and h_2.

The model of the track based on the conventional Timoshenko beam model may be used up to about 2000 Hz [8].

The wheel is regarded as a loaded mass which moves along the rail at a constant V speed. Wheel mass is M_w and the load force P_0.

The wheel/rail contact is modelled as a spring between the wheel and the rail. The wheel/rail contact force $P(t)$ is related to the wheel/rail deflection, according to Hertz's theory.

The equations of motions are

- for the track

$$\mathbf{L}_{x,t}\{\mathbf{q}\}+\sum_{i\in Z}\left(\mathbf{A}_t\{\mathbf{q}_i\}+\mathbf{B}_t\{\mathbf{q}_i^s\}\right)\delta(x-s_i)=\{\mathbf{p}\} \tag{1}$$

$$\mathbf{C}_t\{\mathbf{q}_i^s\}=\mathbf{D}_t\{\mathbf{q}_i\} \tag{2}$$

where $\mathbf{L}_{x,t}$, $\mathbf{A}_t$, $\mathbf{B}_t$, $\mathbf{C}_t$ and $\mathbf{D}_t$ stand for matrix differentials (see appendix [7]), $\{\mathbf{q}\} = \{\mathbf{q}(x, t)\} = [u(x, t)\ v(x, t)\ \theta(x, t)]^T$ is the column vector of rail displacements, $\{\mathbf{q}_i\}=\{\mathbf{q}(s_i, t)\}$, $\{\mathbf{q}^s{}_i\} = \{\mathbf{q}^s{}_i(t)\} = [x_i(t)\ z_i(t)\ \alpha_i(t)]^T$ is the column vector of the considered i sleeper displacements, $\{\mathbf{p}\} = -P(t)\delta(x- Vt)\{\mathbf{e}\}$ is the column vector of forces on the rail where $P(t)$ is the wheel/rail contact force, $\{\mathbf{e}\} = [\,0\ 1\ 0\,]^T$ and $\delta(.)$ is Dirac's delta function.

- for the wheel

$$M_w \ddot{z}_w(t) = P_0 - P(t). \tag{3}$$

The wheel/rail contact force is expressed by

$$\left[P(t)/C_H\right]^{2/3} = z_\delta(t) H\left[z_\delta(t)\right], \tag{4}$$

where $z_\delta(t) = z_w(t) - v(Vt,t)$ is wheel/rail deflection, C_H represents the Hertzian constant and H[.] is the Heaviside function.

The boundary conditions are

$$\lim_{|x-Vt|\to\infty} \{\mathbf{q}(x,t)\} = \begin{bmatrix}0 & 0 & 0\end{bmatrix}^T, \lim_{i\to\pm\infty} \{\mathbf{q}_i^s(t)\} = \begin{bmatrix}0 & 0 & 0\end{bmatrix}^T \tag{5}$$

and the initial conditions are

$$z_w(0) = 0, \quad \dot{z}_w(0) = 0,$$

$$\{\mathbf{q}(x,0)\} = \begin{bmatrix}0 & 0 & 0\end{bmatrix}^T, \quad \{\dot{\mathbf{q}}(x,0)\} = \begin{bmatrix}0 & 0 & 0\end{bmatrix}^T,$$

$$\{\mathbf{q}_i^s(0)\} = \begin{bmatrix}0 & 0 & 0\end{bmatrix}^T, \quad \{\dot{\mathbf{q}}_i^s(0)\} = \begin{bmatrix}0 & 0 & 0\end{bmatrix}^T. \tag{6}$$

The differential equations of motion may be solved through numerical step-by-step integration, using an original Green functions method. For this aim, the Green function's column vector for rail displacement $\{\mathbf{g}(x, \xi, t - \tau)\} = [g^u(x, \xi, t - \tau), g^v(x, \xi, t - \tau), g^\theta(x, \xi, t - \tau)]^T$ was calculated [7]. Starting to the Green function $g^v(x, \xi, t - \tau)$, the rail displacement at the contact point may be determined

$$\begin{aligned} v(Vt,t) &= -\int_{-\infty}^{\infty}\int_0^t g^v(Vt,\xi,t-\tau)P(\tau)\delta(\xi - V\tau)\mathrm{d}\tau\mathrm{d}\xi = \\ &= -\int_0^t g^v(Vt,V\tau,t-\tau)P(\tau)\mathrm{d}\tau. \end{aligned} \tag{7}$$

The Green function is damped and then,

$$g^v(Vt,V\tau,t-\tau) \cong 0, \tag{8}$$

for a certain T and $t - \tau > T$. Also, the Green function is periodical because the track is a periodical structure

$$g^v\left(V(t+kT_0),V(\tau+kT_0),t-\tau\right)=g^v\left(Vt,V\tau,t-\tau\right), \tag{9}$$

for $t - \tau \in [0, T]$, where $T_0 = d/V$ and k is an integer.

The wheel vertical displacement and speed are

$$z_w(t)=z_w(0)+\int_0^t \dot{z}_w(\tau)\mathrm{d}\tau\,,\quad \dot{z}_w(t)=\dot{z}_w(0)+\frac{1}{M_w}\int_0^t\left[P_0-P(\tau)\right]\mathrm{d}\tau\,. \tag{10}$$

Practically, a certain $t_0, t_1, \ldots t_n$ (with $t_0 = 0$, $t_n = t$ and $\Delta t = t_i - t_{i-1}$ where $i = 1 \div n$) must be considered. The rail displacement at the contact point and the wheel displacement and speed can be calculated with the formulae

$$v(Vt_n,t_n)=-\sum_{i=1}^{n}\int_{t_{i-1}}^{t_i} g^v(Vt_n,V\tau,t_n-\tau)P(\tau)\mathrm{d}\tau \tag{11}$$

$$z_w(t_n)=z_w(t_{n-1})+\int_{t_{n-1}}^{t_n}\dot{z}_w(\tau)\mathrm{d}\tau \tag{12}$$

$$\dot{z}_w(t_n)=\dot{z}_w(t_{n-1})+\frac{1}{M_w}\int_{t_{n-1}}^{t_n}\left[P_0-P(\tau)\right]\mathrm{d}\tau\,. \tag{13}$$

It is assumed that the contact force $P(\tau)$ and the Green function will have a linear variation in the $[t_{i-1}, t_i]$ time interval.

$$\dot{z}_w(t_n)=\dot{z}_w(t_{n-1})+\frac{\Delta t}{M_w}\left[P_0-\frac{P(t_n)+P(t_{n-1})}{2}\right] \tag{14}$$

$$z_w(t_n)=z_w(t_{n-1})+\dot{z}_w(t_{n-1})\Delta t+\frac{\Delta t^2}{2M_w}\left[P_0-\frac{P(t_n)+2P(t_{n-1})}{3}\right] \tag{15}$$

$$v(Vt_n,t_n)=-\Delta t\sum_{j=1}^{n}\left\{\frac{g^v_{j-1}P_j+g^v_jP_{j-1}}{2}+\frac{\left(g^v_j-g^v_{j-1}\right)\cdot\left(P_j-P_{j-1}\right)}{3}\right\}, \tag{16}$$

where $g^v_j = g^v(Vt_n, Vt_j, t_n - t_j)$ and $P_j = P(t_j)$.

Using the above properties of the Green function, $g^v(Vt_n, Vt_j, t_n - t_j)$ can be organized as a matrix – the Green matrix of the track. For any time numerical simulation, the Green matrix of the track can be utilised.

The wheel displacement and the rail deflection can be expressed as functions of magnitude contact force $P(t_n)$. By substituting the wheel displacement and the rail deflection in the contact equation (4), a non-linear $P(t_n)$ based equation results. Solving this equation in an iterative manner, the $P(t_n)$ contact force is determined at each integration step. Then, the wheel displacement and the rail deflection are determined. After that, the procedure repeats with the next step.

2. Numerical application

Further on, the particular case of a moving wheel on the rail track consisting in a rail having the linear mass m = 56 kg/m on concrete sleepers, is analyzed. The wheel mass M_w = 750 kg and a static load P_0 = 100 kN are considered. The values for the rail parameters are: $I = 23.14 \cdot 10^{-6}$ m^4, $S = 7.134 \cdot 10^{-3}$ m^2, E = 210 GPa, G = 85 GPa, $\kappa = 0.34$, M_s = 129 kg, $I_s = 0.82$ kgm^2, $d = 0.698$, h = 0.08 m , h_1 = 0.085 m, h_2 = 0.089 m, k_{rx} = 34 MN/m, k_{rz} = 280 MN/m, $k_{r\alpha}$ = 114.3 kNm, c_{rx} = 24 kNs/m, c_{rz} = 63 kNs/m, $c_{r\alpha}$ = 25.7 Nms, k_{bx} = 35 MN/m, k_{bz} = 180 MN/m, c_{bx} = 52 kNs/m and c_{bz} = 82 kNs/m.

The Hertzian constant $C_H = 11.86\ 10^{10}$ N/m$^{3/2}$ was calculated for a wheel having a 920 mm diameter and an S 78 rolling profile on UIC 56 rail.

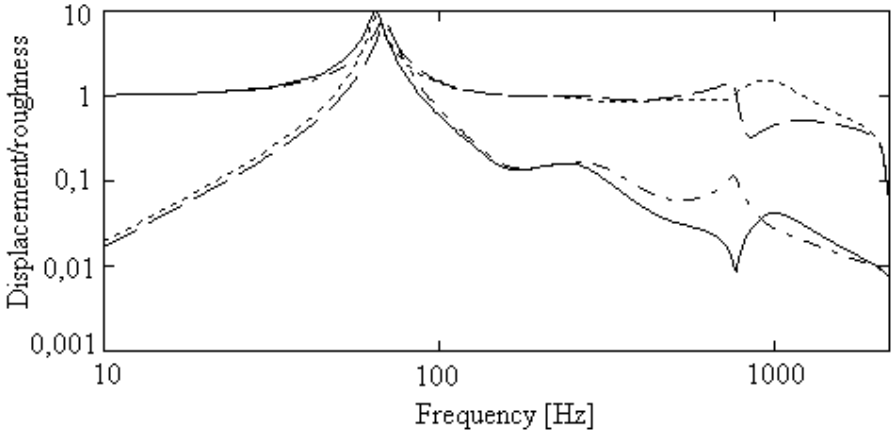

Fig. 2. Wheel/rail response for harmonic behaviour: ——— wheel between sleepers, — · — · — wheel above sleeper, – – – – rail between sleepers, — — — rail above sleeper.

Firstly, in order to understand the wheel/rail interaction due to parametric excitation, the wheel/rail harmonic behaviour is analyzed. For this purpose, the model

of a moving irregularity between a stationary wheel and the rail is adopted. The wheel/rail response is calculated from the equations

$$\frac{\bar{v}}{\bar{z}_r} = -\frac{\bar{\alpha}_r}{1/k_H + \bar{\alpha}_w + \bar{\alpha}_r}, \quad \frac{\bar{z}_w}{\bar{z}_r} = \frac{\bar{\alpha}_w}{1/k_H + \bar{\alpha}_w + \bar{\alpha}_r},$$

$$\frac{\bar{P}}{\bar{z}_r} = -\frac{1}{1/k_H + \bar{\alpha}_w + \bar{\alpha}_r},$$

where $\bar{v}$ and $\bar{z}_w$ are the complex amplitudes of the rail and the wheel, $\bar{P}$ is the complex amplitude of contact force, $\bar{z}_r$ is the complex roughness amplitude, $\bar{\alpha}_w$ and $\bar{\alpha}_r$ are the wheel and rail receptances and k_H is the elastic constant of the Hertzian contact.

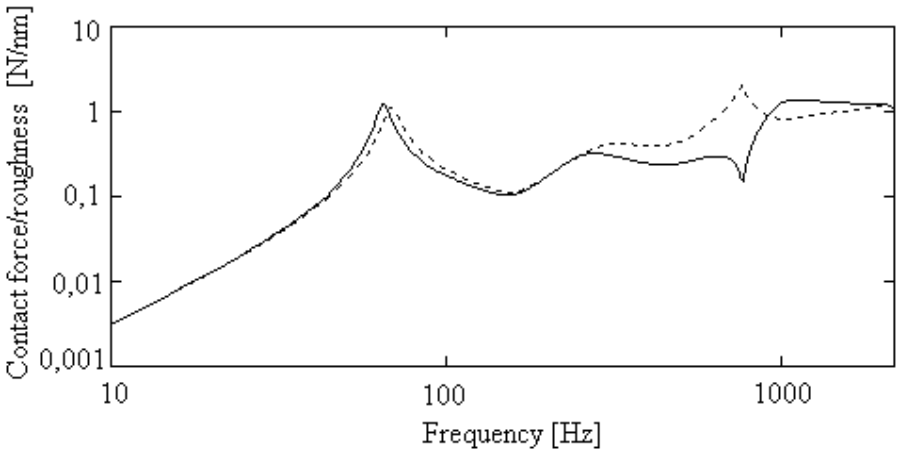

Fig. 3. Wheel/rail contact force for harmonic behaviour: ——— at mid-span, — — above sleeper.

Fig. 2 and 3 display the wheel and rail displacement, respectively the contact force in the domain of 10 - 2200 Hz. All values are compared to the roughness. Two resonances may be observed, the first at frequency about 65 Hz, and the second at frequency about 240 Hz. The rail displacement is smaller than the wheel's in the frequency range below the first resonance because the rail receptance is smaller than the wheel's. After the first resonance, the wheel receptance is smaller and its displacement is smaller too.

The pinned-pinned resonance/anti-resonance occurs at a frequency of about 760 Hz. The rail resonance and the wheel anti-resonance are connected, and the rail

anti-resonance and the wheel resonance are connected too. The contact force diagram shows that the differences between the system's response above a sleeper and at mid-span are maximal at the pinned-pinned resonance/anti- resonance frequencies.

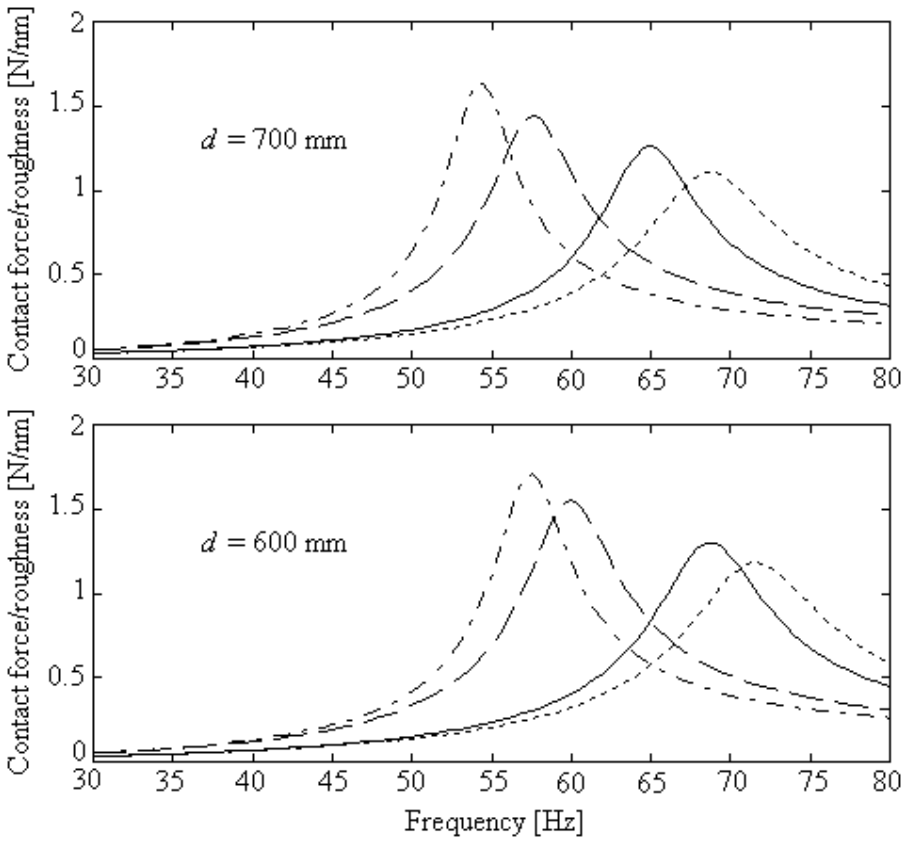

Fig. 4. Contact force: wheel mass of 750 kg, ——— at mid-span, – – – – above sleeper, wheel mass of 1100 kg, — · — · — at mid-span, — — above sleeper.

Fig. 4 shows the contact force around the first resonance frequency for two wheel masses, 750 kg and 1100 kg, and for two span lengths 700 mm and 600 mm. The first resonance frequency varies with a few Hz for the wheel between sleepers or above the sleeper. If the wheel mass is 1100 kg, then the first resonance frequency decreases with about 11-12 Hz comparing with the wheel mass of 750 kg, and the contact force increases with about 0,34-0,37 N/nm. The first resonance frequency increases slightly with 2,5-3,5 Hz for a span length of 600 mm comparing with the span length of 700 mm.

In the following, the numeric simulation results in the time-domain are analyzed. The track Green matrix was calculated for many speed values between 20 m/s and 60 m/s, both for span length of 700 mm and 600 mm. In order to capture the high frequency dynamic response, the time step for integrating the equations of motion was chosen between 16.67 and 50 μs.

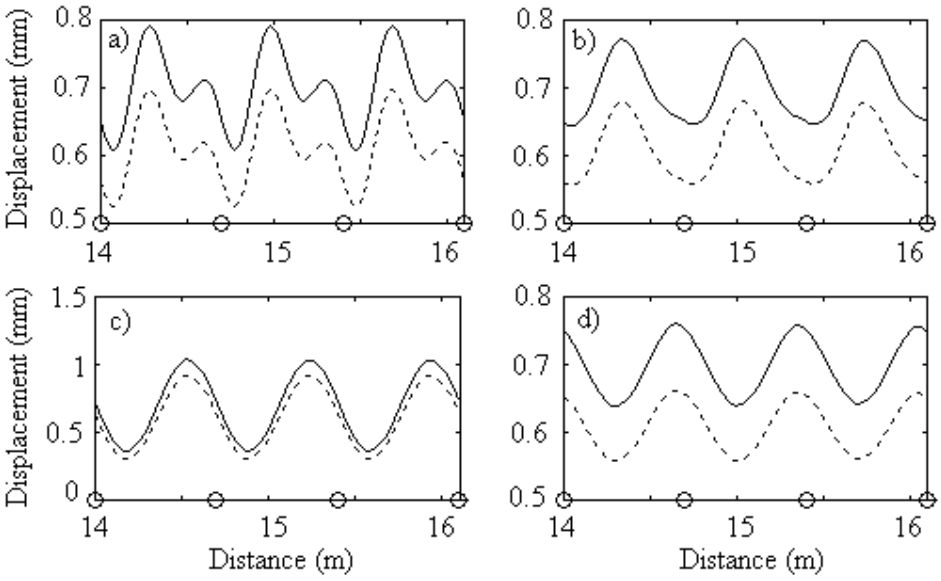

Fig. 5. Wheel/rail displacement at the contact point: a) at 24 m/s, b) at 28 m/s; c) at 48 m/s, d) at 60 m/s; ——— wheel displacement, – – – – rail displacement, ○ sleeper position.

Fig. 5 displays the displacement of the wheel and the rail at the contact point in the interaction due to parametric excitation, between sleepers # 20 and # 24, at different speeds. The displacement of the wheel is larger than the rail's because the wheel/rail contact is elastic. The displacements of the wheel/rail system are higher at the speeds of 24 m/s and 48 m/s especially. At the wheel speed of 48 m/s, the frequency of passing over sleepers (the first spectral component of wheel/rail interaction due to parametric excitation) equals the first resonance frequency, and this fact counts for the magnitude of displacements. This speed value may be named the critical speed of wheel/rail interaction due to parametric excitation. At the wheel speed of 24 m/s, the second spectral component of wheel/rail interaction due to parametric excitation equals the first resonance frequency too. This aspect explains the double oscillation of wheel/rail displacements along the sleeper bay. At the speeds equal the critical speed of wheel/rail interaction due to parametric excitation, the minimal wheel/rail

displacements may be observed after the wheel passes over the sleeper, especially when the wheel speed is higher than the critical speed.

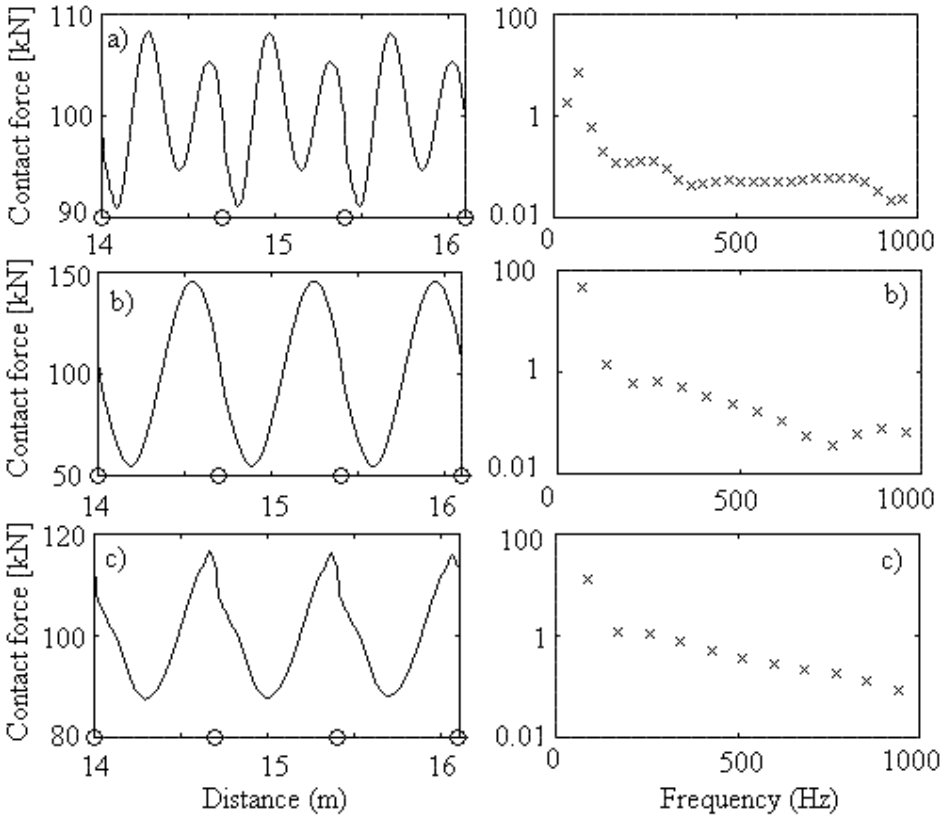

Fig. 6. Wheel/rail contact force: a) at 24 m/s, b) at 48 m/s, c) at 60 m/s, —— contact force, × spectral component, ○ sleeper position.

Fig. 6 presents the wheel/rail contact force for time-domain and its spectral components. The numerical simulation shows that the contact force above sleeper increases with the speed. Generally, the spectrum of the contact force is dominated by the first component which has the frequency equal to the frequency of passing over the sleepers. The first two components have the magnitude of 45.7 kN and 1.4 kN at 48 m/s, and 12.6 kN and 1.2 kN at 60 m/s, respectively. There is an exception, when the wheel speed is about half the critical speed. In this case, the second spectral component is the highest, e.g. it has the amplitude of 7.0 kN and the first spectral component, 1.9 kN at the wheel speed of 24 m/s. On the other hand, the highest spectral components increase as the wheel speed increases.

Fig. 7 displays the effective contact force for the wheel mass of 750 kg and 1100 kg, for both the span length of 700 mm and 600 mm. One can see the critical speed in every studied case. Thus, the critical speed decreases as the wheel mass increases because the first own wheel/rail resonance frequency decreases. Such as, the critical speed is 48 m/s for the wheel mass of 750 kg and 40 m/s for wheel mass of 1100 kg, respectively and the span length of 700 mm. The same trend can be observed for the span length of 600 mm, the critical speed is 43 m/s for a wheel mass of 750 kg and it decreases to 36 m/s for the wheel mass of 1100 kg. Comparing these numerical results one can conclude that the critical speed decreases as the span length decreases as well.

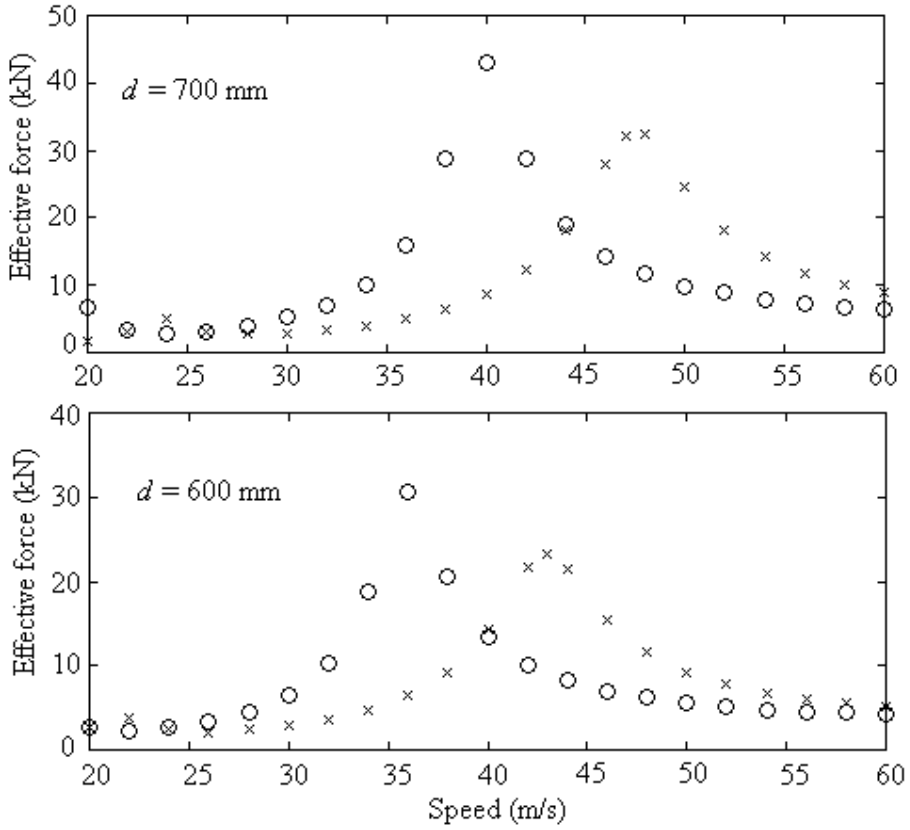

Fig. 7. Effective wheel/rail contact force: × wheel mass of 750 kg, ○ wheel mass of 1100 kg.

In fact, if the wheel rolls over a smaller span length, the frequency of passing over the sleepers is higher. On the other hand, the first own wheel/rail frequency increases as the span length decreases because the stiffness per unit length increases. However, the slope of the frequency of passing over the sleepers

is higher than the first own wheel/rail frequency's and, as the result, the critical speed decreases.

The effective force has its maximum value at the critical speed. The critical value of the effective force increases with wheel mass. Indeed, when the wheel mass is heavy, then the own first wheel rail frequency is smaller and the damping force is smaller too. Because of this, the effective force increases: starting from 32.4 kN to 43.1 kN for the two wheel masses and the span length of 700 mm, and starting from 23.3 kN to 30.7 kN value for the span length of 600 mm. Finally, the critical effective force decreases when the passing time over the sleepers becomes smaller.

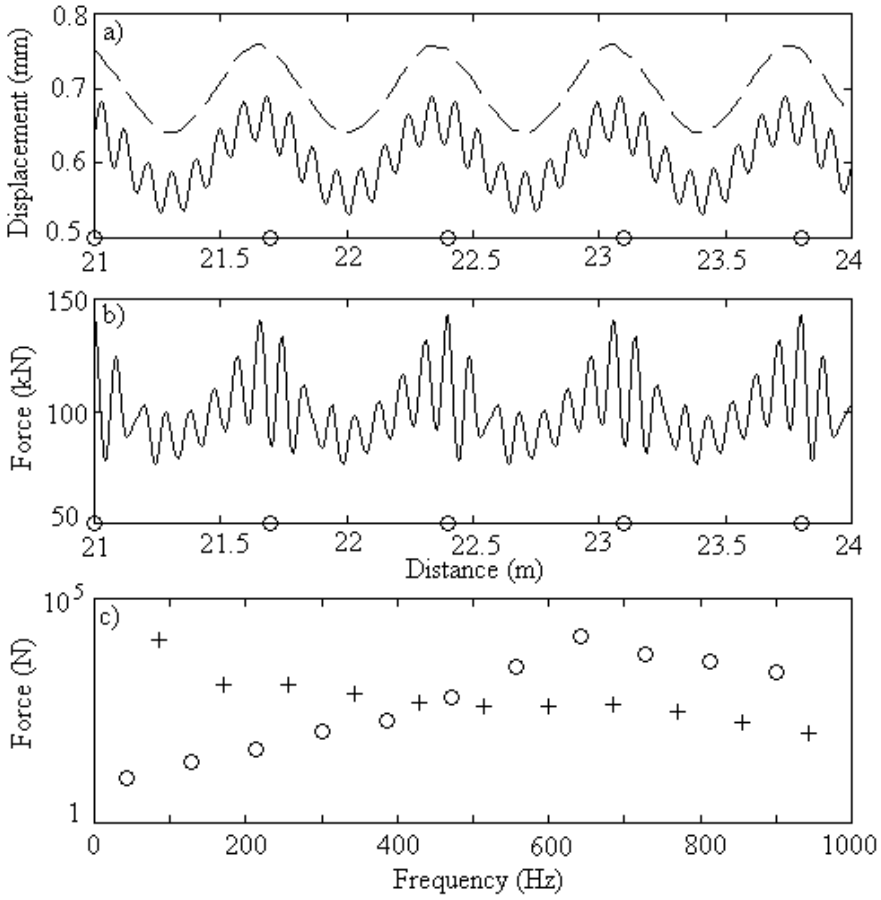

Fig. 8. Wheel/rail response due to harmonic excitation by the wavelength of 93.33 mm at wheel speed of 60 m/s: a) —— rail displacement, – – – wheel displacement, ○ sleeper position; b) contact force; c) contact force spectrum, ○ modulated components, + components due to parametric excitation.

Figure 8 displays the wheel/rail response due to parametric excitation and the rail roughness input at the wheel speed of 60 m/s. For numerical simulation, the term of the rail roughness must be added in the equation (4). The rail roughness has sinusoidal form with the amplitude of 30 μm and wave length of 93.33 mm. The rail displacement is modulated by the roughness because the rail receptance is smaller than the wheel's and the rail compensates the roughness by its displacement.

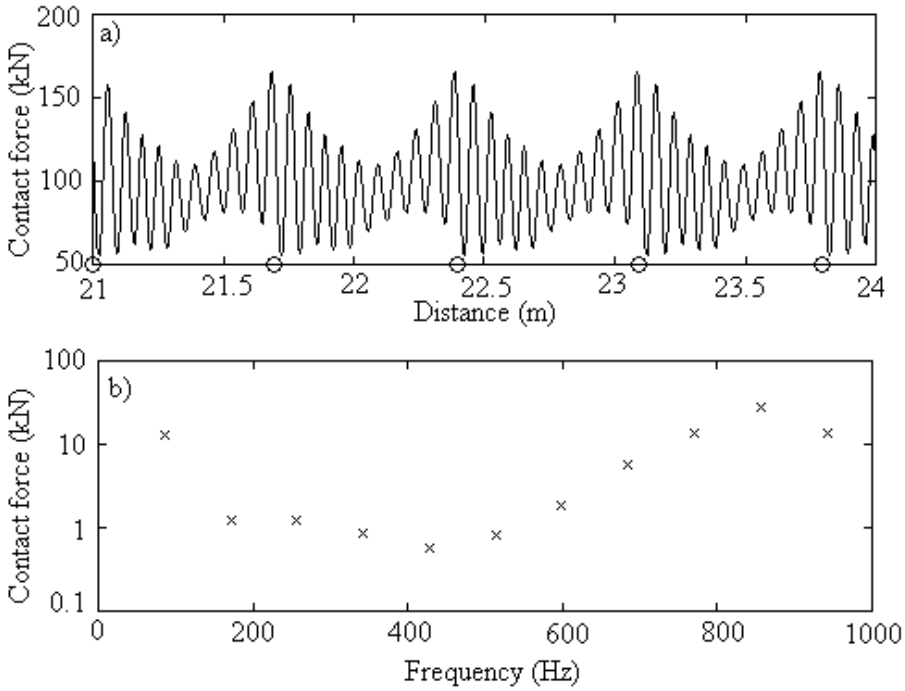

Fig. 9. Wheel/rail contact force due to harmonic excitation by the wavelength of 70 mm, wheel speed = 60 m/s: a) contact force; b) contact force spectrum.

The contact force is modulated too as it can be seen. In fact, the wheel/rail response due to parametric excitation is overlapped by the wheel/rail response due to roughness. In this case, the carrier frequency is caused by the sinusoidal roughness excitation and the modulated one is given by the interaction due to parametric excitation. The carrier has 643 Hz and the fundamental component of the modulated has 86 Hz. The spectrum of the contact force has two distinctive components: the harmonics of the modulated and the modulated spectral components with the frequencies of $f_c \pm k\, f_m$ where f_c stands for the frequency of the carrier, f_m stands for the frequency of the modulated and k stands for an integer number. The amplitude of the carrier has the value of 14.6 kN and the amplitude

of fundamental component has the value of 12.5 kN. The effective force has the value of 14.8 kN.

When the carrier frequency is a multiple of the fundamental component of the interaction due to parametric excitation, both kind of components are overlapped. Figure 9 illustrates this aspect, the contact force and its spectrum due to roughness with the wavelength of 70 mm and the same amplitude and wheel speed are presented. The amplitude of the fundamental modulated has the value of 12.6 kN and the carrier one has the value of 28.1 kN. The effective force has the value of 26.3 kN. The modulated fundamental is practically unaffected by the carrier. In this last case, the frequency of the carrier is situated in the pinned-pinned range and the contact force is higher.

3. Conclusions

In the case of ballasted track on sleepers, the wheel/rail interaction is strongly influenced by the parametric excitation due to sleepers, the dynamic stiffness of the track varying along the span bay.

This particularly type of wheel/rail interaction behaviour must be studied for many reasons (wheel/rail wear, the rolling noise, etc.). For this aim, an original theoretical model is presented. The rail is assumed as an infinite Timoshenko beam, respectively an infinite bar which are coupled by the rail–pads. The wheel is taken as a moving mass on the rail. In order to simulate the wheel/rail interaction, an efficient method based on the Green matrix of the track is applied.

The wheel/rail interaction behaviour due to parametric excitation is dominated by the first own frequency for wheel/rail system. When the passing frequency over the sleepers equals the first own resonance frequency, the wheel/rail contact force due to parametric excitation has the highest value and the wheel rolls over the rail at the critical speed. Consequently, the railway traffic at the critical speed must be avoided.

The numerical results show that the wheel/rail contact force may be reduced if the railway vehicle has the light wheel sets. In addition, the wheel rolling on a track with smaller span length is less stressed.

As the wheel speed increases, a part of the main components of the contact force spectrum due to parametric excitation are pushed in the pinned-pinned resonance frequency range and the amplitudes of these spectral components become higher. The previously mentioned aspect contributes to the rail corrugation.

Generally, the wheel/rail interaction is characterised by the superposition of the roughness and parametric excitation due to sleepers. The modulated oscillation phenomenon occurs – the carrier is the effect of the excitation due to roughness and the modulated is given by the parametric excitation. The spectral

components of both the carrier and the modulated can be added in the pinned-pinned resonant/anti-resonant frequency range, especially. As a result, the contact force becomes higher, and this last aspect contributes to the rail corrugation too.

R E F E R E N C E S

[1]. *Nordborg, A.* Wheel/rail noise generation due to nonlinear effects and parametric excitation, Journal of the Acoustical Society of America 111 (2002) 1772-1781.
[2]. *Hou, K., Kalousek, J., Dong, R.* A dynamic model for an asymmetrical vehicle/track system. In: Journal of Sound and Vibration 267 (2003) 591-604.
[3]. *Wu, T. X., Thompson, D.J.* On parametric excitation of the wheel/track system. In: Journal of Sound and Vibration 278 (2004) 725-747.
[4]. *Clark, R. A., Dean, P.A., Elkins, J.A., Newton, S. G*. An investigation into the dynamic effects of railway vehicles running on corrugated rails, Journal Mechanical Engineering Science 24, 1982, 65-76.
[5]. *Nielsen, J.C.O., Igeland, A.* Vertical dynamic interaction between train and track- influence of wheel and track imperfections, Journal of Sound and Vibration 185, 1995, 825-839.
[6]. *Mazilu*, *Tr*. Propagation of harmonic vertical waves in a rail, *Scientific Bulletin Series D: Mechanical Engineering*, vol. 67 no. 2 (2005) 99-110.
[7]. *Mazilu, Tr.* The rail's response to the action of vertical sliding force. In: Scientific Bulletin Series D: Mechanical Engineering, vol. 68 no. 2 (2006) 41-58.
[8]. *Wu, T.X., Thompson, D.J.* A double Timoshenko beam model for vertical analysis of railway track at high frequencies, Journal of Sound and Vibration 224 (1999) 329-348.